Low thermal emissivity coating based on aluminium / acrylic composite coatings

Low thermal emissivity coating based on aluminium / acrylic composite coatings

E E Ateia[1], M A Metwaly[1], H R Tantawy[2]

[1] Physics Department, Faculty of Science, Cairo University, Giza, Egypt
[2] Chemical Engineering Department, Military Technical College (M.T.C)

E-mail: cap.mahmoud2011@gmail.com

Abstract. Low emissivity coatings were synthesized by using fine flake Aluminium (Al) powder as a filler within acrylic resin to from the desired composite coatings. In the current work, ball milling was applied to prepare Al with different shapes and sizes. The technical parameters of prepared Al powders with respect to the initial raw Al are characterized by scanning electron microscope (SEM), X-Ray diffraction (XRD), and Energy Dispersive X-Ray Analysis (EDX). Moreover, parameters that affect the emissivity of the coating was investigated; such as coating thickness, particle size, spin coating, ball milling time and the content of coated Al powder. The thermal signature is highly affected by the variation in Al content (5%, 20%, 25%, 35%, 40% and 60%) at different temperatures (50ºC, 70ºC, 90ºC). The results indicate that the perfect percentage for the filler (Al) in the matrix within the range (35 wt. - 40 wt. %) and Al fine flake powder particle, which gives the lowest infrared emissivity of 0.385 µm and 0.412 µm for (3-5) µm, (8-12) µm, respectively.

1. Introduction

Two main goals for the art of military camouflage. Firstly, concealing a possible target such as building, aircraft, tank, weapon emplacement. Secondly, simulating a false target or decoy to divert attention away from real targets [1]. Previously, camouflage nets or mats were used to conceal the target by covering it and were only intended to prevent visual target detection by providing an image that was dissimilar to that of the surrounding terrain. This Simple visual camouflage formed of a covering surface that was painted on and otherwise designed to look like a normal product or terrain surface while concealing the target underneath it [2, 3]. Minimizing external heat absorption and reducing intensity of infrared radiation emitted by military targets can be achieved by using Low-emissivity materials [4]. Low infrared emissivity coatings have attracted a lot of interest because of their military and civilian purposes, such as infrared camouflage, energy saving, and vehicles protection from infrared detection [5, 6]. The infrared Emissivity should be as low as possible in order to achieve excellent IR camouflage efficiency [4]. With the increasing development of infrared detection techniques and infrared guided weapons low infrared emissivity have been achieved by using different types of materials such as composite ceramic[7-9], bio-electret composites [10, 11], and metals such as silver and aluminum [12-15], AlSiN and Ag-alloy multilayer films [16]. In general, metallic pigments, polymer binder, organic solvent and additives are the mainly composition for preparing low infrared emissivity coatings [17-19]. While visual camouflage is still important, the production of other types of military sensing and visibility devices has complicated the requirement for concealment. Older types of camouflage can be ineffective against radar surveillance and interrogation systems which use electromagnetic wavelengths in the infrared and ultraviolet bands [20]. Infrared sensors sense heat (infrared) radiation generated by

exhaust system and hot engine of the machines, this heat arises from unprotected and running military tank or truck. when the target concealment is the aim, understanding the terrain characteristics (e.g. snow, farmland, marsh, desert, woods etc.) is important if the risk of target detection is to be minimized [21]. The camouflage should reduce or remove contrast between the target and the surrounding terrain, eliminate transmission of energy (e.g. far infrared) emanating from the target, and reflect, scatter, or absorb incoming target illuminating energy beams (e.g. , laser coherent, sunlight, radiation, radar, etc.) in a manner that mimics the return or signature of the surrounding terrain [22].

2. Materials and Method

2.1 Materials.

Al powder (fine powder, purity 99.5%, 35µm) was purchased from Alpha Chemika (India). Solvents such as toluene (>99%) and ethanol (≥99.5%) were purchased from Al-Ahram Chemicals (Egypt). Commercial acrylic coat was purchased KAPCI coatings company (Egypt), it consists mainly from clear coat (Kapci 3100 2k MS) and hardener (kapci MS 651) with optimum mixing ratio (2:1). The resultant acrylic coat delivers high gloss, excellent finish, weathering resistance and offers high durability.

2.2 Preparation of controlled particle size Al Powder.

The high energy ball milling (Fritsch GmbH, Milling and Sizing, Industriestrasse8, 55743 Idar-Oberstein. Germany) was utilized for preparing of flake Al. The ratio between initial Al fine powder and milling balls during the preparation period was fixed at 1:15. Typically, 15g of Al powder with 225 gram balls were milled for 30 hours at steady speed of 350 rpm in a wet medium of 70 ml of toluene. The crucial rule of toluene was to prevent oxidation and agglomeration of powder. Moreover, milling was carried out interrupted cycle involving 15 min on and 30 min off for an effective time of 15 and 30 hours. The samples were taken at different times (0, 15, 30 hours) to inspect the impact of milling time on Al particle size and shape. Details of milling process were summarized in Table (1).

2.3 Preparation of Al/ acrylic composite coatings.

teel substrates (10 cm×10 cm, thickness 1.0 mm) were used to test the variations in the emissivity after the application of various coatings as shown in Fig. (1). All the substrates were pretreated with 10% dilute H2SO4 then distilled water at ambient temperature before applying the desired coating. Moreover, fixed amounts of polymer (clear coat, hardener) and Al powder were mixed together under continuous ultra-sonication for 10 min in order to prepare the Al/ acrylic composite coatings suspensions. The ratio between clear coat and hardener about (2:1) according to kapci coatings company regulations. Then the obtained coatings suspensions mixtures was painted onto the steel substrates via a spin coater technique (KW-4A, U.S.A.). Spin coater was adjusted at two speeds, low speed (speed 1) up to 2500 rpm and high speed (speed 2) up to 8000 rpm. Finally, the coatings were solidified completely after curing for 24 h at room temperature and kept for further characterization.

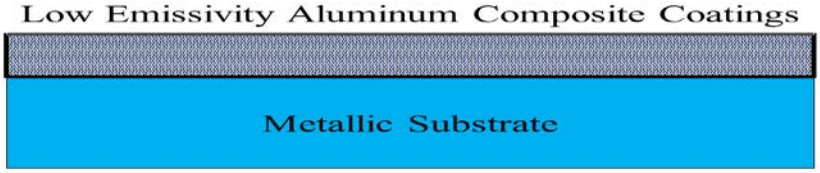

Figure 1. The schematic diagram of the low emissivity coating.

Table 1. Milling conditions and details of planetary ball mill

No	Parameter	Value
1	Rotation speed of vial (rpm)	350
2	Capacity of vial (ml)	500
3	Vial material	Zirconium oxide
4	Ball material	Zirconium oxide
5	Diameter of ball(mm)	10
6	Ball to powder weight ratio	15:1
7	Times of milling (h)	0-30
8	Types of milling	Wet
9	Process control agent	Toluene
10	Initial powder mass (g)	15

3. Characterizations

Morphological characterization and particle size analysis of the Al samples were carried out by scanning electron microscope (SEM, MIRA 3 XMU, TESCAN). The powder was suspended in ethanol. The suspension was ultrasonicated for 20 minutes and waiting until it dries. The dried samples were then mounted on to a SEM sample stub. X- Ray diffractometer (XRD, ADX 2500) with Cu Kα radiation source was utilized to examine the crystallinity and investigate the impact of milling process on crystallinity of Al. The Elcometer 456 (England) coating thickness gauge scan probe was used for drying film thickness. ET-10 (Surface Optics Corporation 410-0045 ET10, China) used to measure infrared emissivity values within spectral regions 3 -5 and 8 -12 μm. The thermal signature was captured using a fluke thermography (Model: Fluke Ti25 thermal imager, accuracy: ± 2 ºC, Measurement temp range: -20 ºC to +350 ºC, Germany)

4. Results and Discussion

4.1 Morphological analysis.

The impact of milling time (0-30h) on the shape and size of the ball milled synthetized Al powders was investigated with SEM as shown Fig. (2). The SEM images represent the variation of the grain sizes with ball milling time. Typical initial Al powder with size around 35μm lateral length flakes as shown in Fig. (3-a). During milling initial Al powder loss its morphology and transformed to irregular-size particle. The observed particles size for 15h and 30h milling were 3μm and ~300nm, respectively as shown in Fig. (3-d) and (3-c). It is clear that the size of the samples is significantly affected by milling time. The amount highly flake Al, decreases with increasing the milling time. It is obvious that flake size decreases to the nano flake size (~300nm) with increasing milling time till 30h. Table (2) represents the variation of average grain size with ball milling time for Al powder.

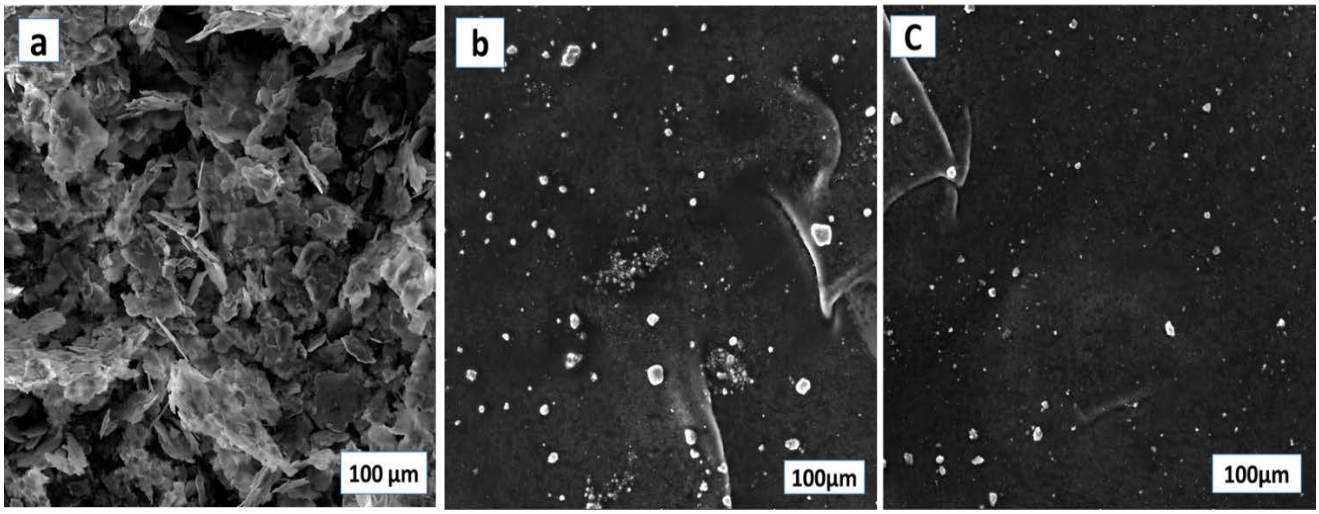

Fig 2. SEM images Al powder samples after milling 0h (a), 15h (b), and 30h (c)

Table 2. Variation of average grain size with ball milling time for Al powder

Ball milling time (h)	Grain size (µm) from SEM
0	35
15	3
30	0.3

4.2 *Energy Dispersive X-ray (EDX) analysis.*

EDX analysis was carried out to examine the degree of oxidation of the obtained samples. EDX analysis of the prepared samples for Al powder is shown in Fig. (3). It elucidates the impact of milling time on the oxidation degree of the samples. Inset of figures shows the relative abundance, between Aluminum and oxygen as a function of the milling time. It is obviously recorded that the oxygen content increases with increasing milling duration. The formation of Aluminum oxides (Al_2O_3) during milling is expected. It is found that by increasing milling time from 0h to 30h. The oxygen content increases from 11% to 39%. In this case, the highest increase in oxygen content is obtained at milling time 30h.

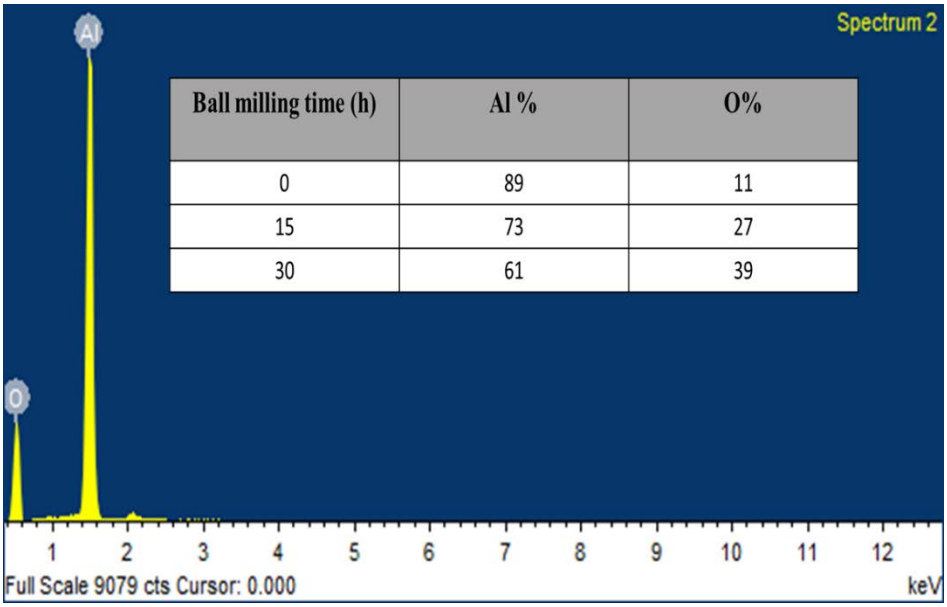

Ball milling time (h)	Al %	O%
0	89	11
15	73	27
30	61	39

Figure 3. EDX of Al powder samples after milling 0h, 15h, and 30h

4.3 *X-ray analysis.*

Figure. (4) Shows the XRD patterns of the ball milled synthesized Al flake samples compared to the starting raw of Al. The sharp diffraction peaks are detected at 2θ values of 38.5o, 44.7o, 65.1o and 78.2o corresponding to (111), (200), (220) and (311) planes respectively. The obtained structure fully matches with diffraction file (JCPDS card No. 99-0005) [23, 24]. Additionally, a diffraction peak appears at 30.4o, 33.6o and 55. 9o corresponding to aluminum oxide (Al_2O_3). The obtained data shows that the increase of the milling time increases the percentage of the aluminum oxide (Al_2O_3) which is clearly detected. The appearance of aluminum oxide (Al_2O_3) starts after 15h of milling. The high increase in the percentage of the aluminum oxide (Al_2O_3) with increasing milling time from 15h to 30h. The obtained data is in a good agreement with EDX analysis.

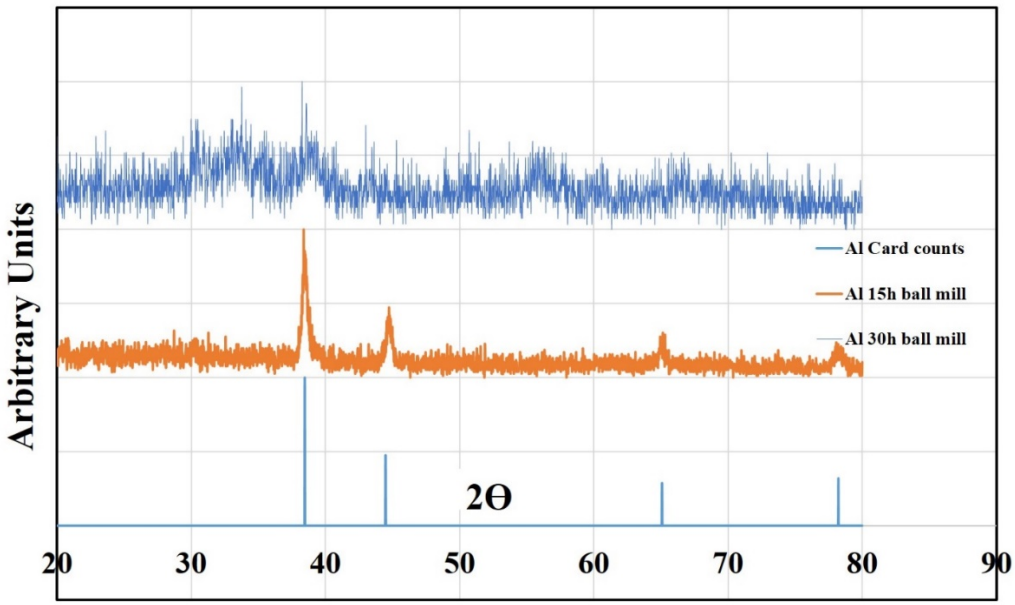

Figure. 4. X-ray diffraction patterns of synthesized Al samples with different milling times

4.4 Factors affecting emissivity.

4.4.1 Coating efficiency. Figure.(5) illustrates the relation between thickness (µm), emissivity (3-5, 8-12µm) and spin coating operational conditions (rpm) where the percentage between the Al powder and the polymer is (1: 9) g. As shown from the figure, the thickness of the coating slightly decreases from 13µm to 10µm with increasing speed (rpm). The infrared emissivity very slightly increases with decreasing thickness and could see that the infrared emissivity nearly at constant value. Therefore, depending on the visual inspection for samples instead of depending on the infrared emissivity at the wavelength of (3-5 µm, 8-12 µm). Figure (6: a-d) shows the dependence of the visual inspection of the samples on the spin coating operational condition (rpm). The difference between the images of the spin coater conditions (rpm) of speed1 and speed 2 is clearly observed. Fixing speed1 at 2, speed2 at 1 and the visual inspection of sample (1) is ok as shown at Fig 6.a. fixing speed1 at 8, speed2 at 1and the visual inspection of sample (4) is ok as shown at Fig 6.b. but sample (1) is more smoothing than sample (4). Fixing speed1 at 2, speed2 at 3 and the visual inspection of sample (5) is not ok as shown at fig 6.c. fixing speed1 at 8, speed2 at 3 and the visual inspection of sample (8) is not ok as shown at Fig 6.d. it was found that by increasing spin coater conditions (rpm) to a high speed where fixing speed2 at 3, the visual inspection of the samples shows that the samples are not smooth, becomes rougher so that the visual inspection of samples (5-8) are not ok as shown at table 3 and the infrared emissivity of this samples slightly increase as the samples becomes rougher. Therefore, the optimum spin coater conditions for commercial resin (clear coat & hardener)/10% Al coatings will be fixed with speed1 (low speed) at 2, time 18 sec, 0.8*1000 rpm and Fixing speed 2 (high speed) at 1, time 20 sec, 1.54*1000 rpm.

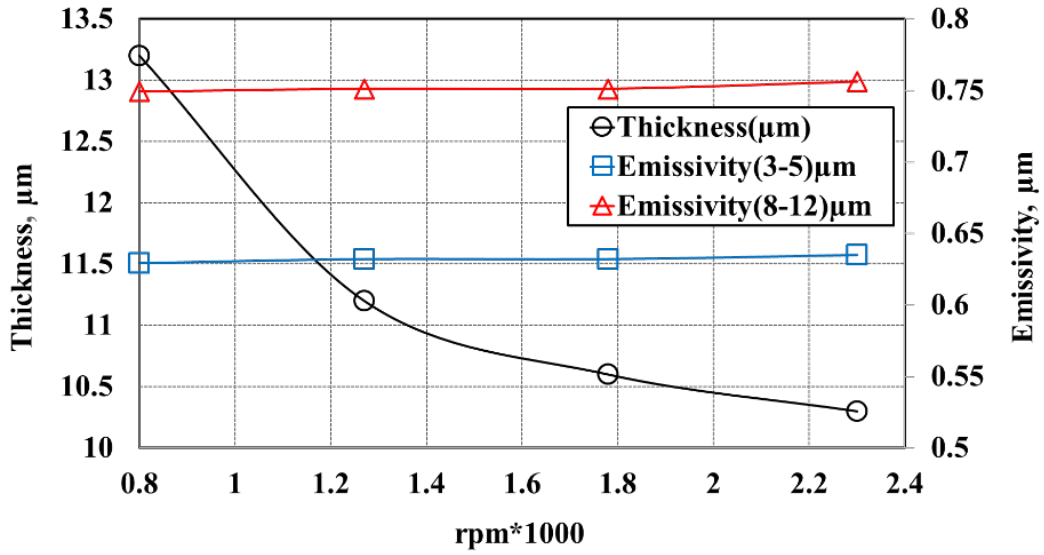

Figure 5. Emissivity at the wavelength of (3-5 µm, 8-12 µm.) and thickness (µm) dependence on spin coating operational condition (rpm).

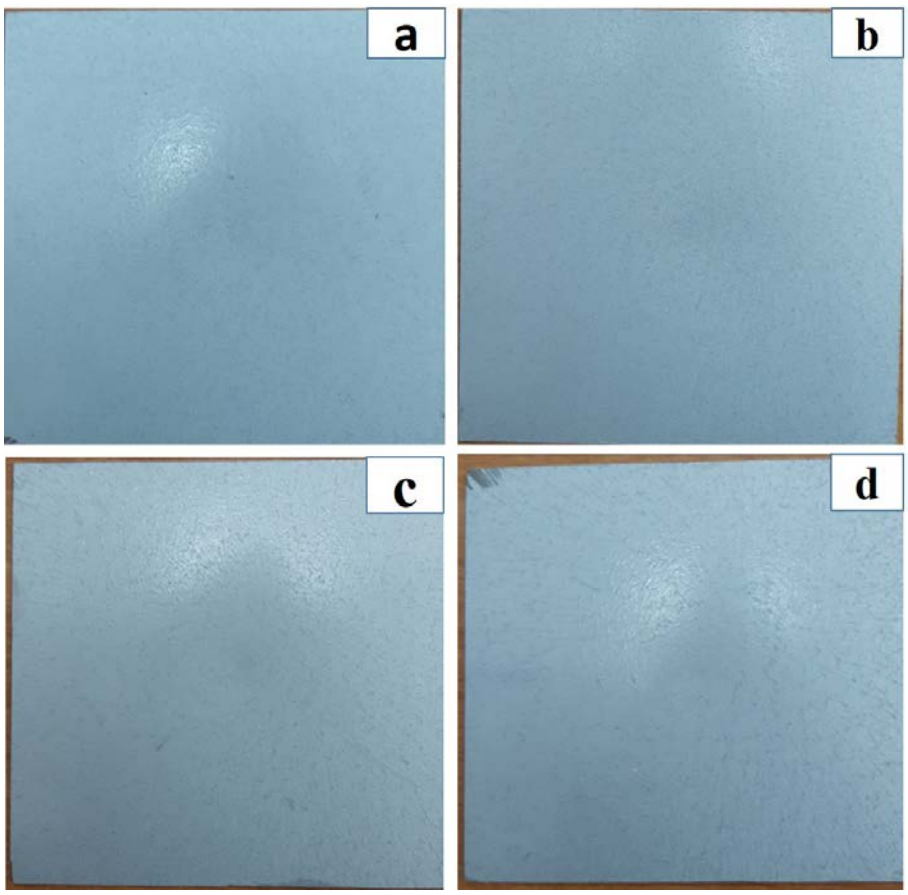

Figure (6: a-d). Shows the visual inspection of samples dependence on spin coating operational condition (rpm) where samples as 10*10 cm

Table 3. The complete set of spin coating operational condition (rpm).

Sample ID	speed 1	Rpm*1000 of speed 1	Speed 2	Rpm*1000 of speed 2	Thickness (µm)	Emissivity (3-5)µm	Emissivity (8-12)µm	Visual inspection
1	2	0.8	1	1.54	13.2	0.629	0.749	ok
2	4	1.27	1	1.54	11.2	0.632	0.751	ok
3	6	1.78	1	1.54	10.6	0.632	0.751	ok
4	8	2.3	1	1.54	10.3	0.635	0.756	ok
5	2	0.84	3	3.01	9.7	----	-----	not ok
6	4	1.3	3	3.01	9.2	-----	----	not ok
7	6	1.75	3	3.01	8.6	----	----	not ok
8	8	2.32	3	3.01	8.2	-----	------	not ok

4.4.2 The effect of thickness on the emissivity of commercial resin/Al composite coatings. In general, the yield of thickness with any composite coatings is nearly fixed and therefore different thickness can't be obtained. To solve this problem, one layer can be coated on the substrate, and then after a few minutes another layer can be coated, etc. waiting for long time can lead to separating the coats. Due to the

previous action, the effect of coating thickness can be examined. Figure. (7) Shows the thickness dependence of infrared emissivity of commercial resin /10% Al coatings where fixing speed1 (low speed) at 2, time 18 sec, 0.8*1000 rpm and Fixing speed 2 (high speed) at 1, time 20 sec, 1.54*1000 rpm. As shown from the figure, when the thickness increases from 13µm to 39µm, the infrared emissivity very slightly decreases from 0.629µm to 0.623µm and from 0.74µm to 0.743µm at two regions (3-5, 8-12) µm. respectively. Therefore, the emissivity profile becomes nearly steady as the thickness reaches 40 µm. With the successive increase of the thickness from 39µm to 115µm, the infrared emissivity increases from 0.623µm to 0.641µm and from 0.743µm to 0.774µm at two regions 3-5 µm and 8-12 µm, respectively. Finally, the optimum thickness for commercial resin (clear coat& hardener) /10% Al coatings is found to be from 13 µm to 39µm.

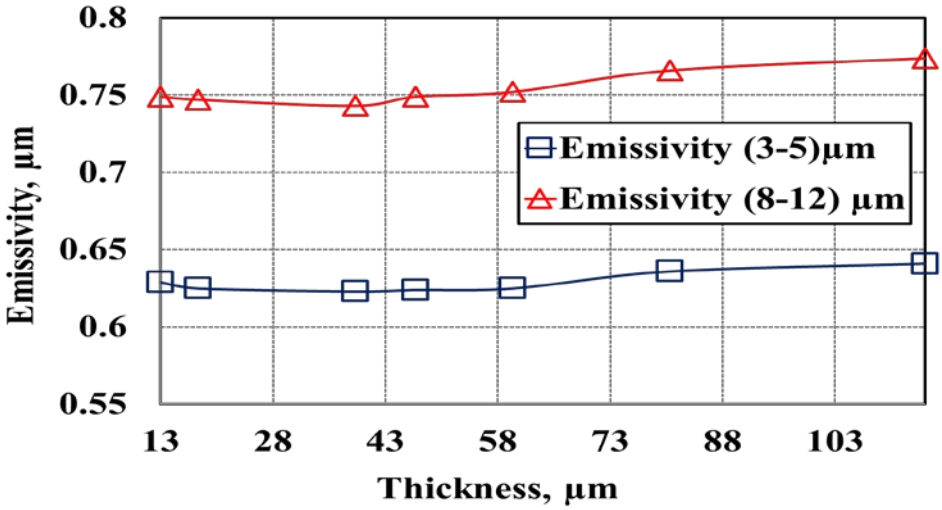

Fig 7. Relation between thickness (µm) and infrared emissivity radiation in two regions (3-5, 8-12) µm

4.4.3 The effect of Al powder content on the emissivity of commercial resin /Al composite coatings. Figure. (8) Shows the relationship between the infrared emissivity of commercial resin/ Al coating and concentration of Al powder. As shown from the figure the infrared emissivity (at band 3-5µm and 8-12µm) of the samples has the same behavior and can be divided into three regions. In the first region, the percentage of Al powder in the mixture is low (5 to 20 wt. %.), hence there are inter distance between the coated Al particles and increase the porosity between particles makes them low reflective to the incident radiation. Therefore, the infrared emissivity decreases with little percentage from values of 0.634µm to 0.589µm and from values of 0.784µm to 0.660µm at two regions 3-5 and 8-12 µm, respectively.

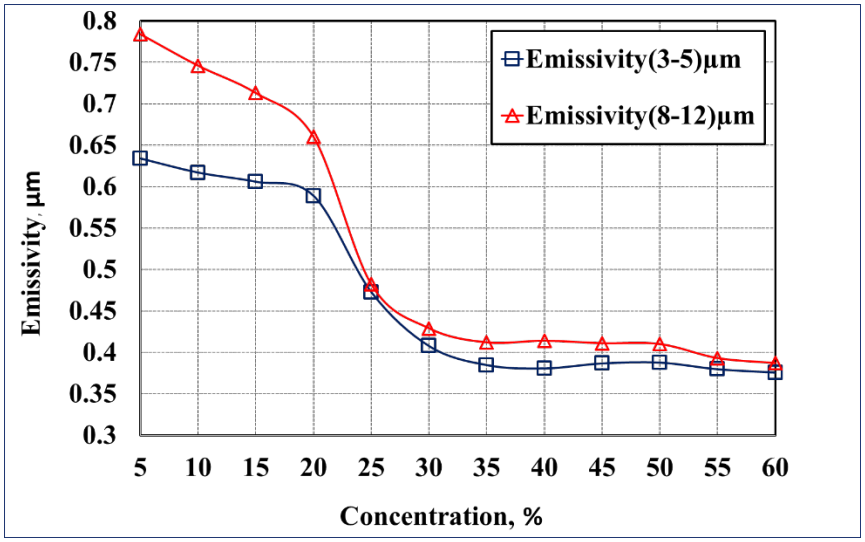

Fig 8. The relation between Al content and infrared emissivity radiation at two regions (3-5, 8-12 µm)

In the second region, the infrared emissivity sharply decreases with increasing the Al content from 20 wt. % to 35 wt. %. Infrared emissivity measurement shows that the emissivity of the coatings sharply decreased from values of 0.589µm to 0.385µm and from values of 0.660µm to 0.412µm at two regions 3-5 µm and 8-12 µm, respectively. High Al content causes the closer packing of the coated Al particles and reduces the porosity between particles making them highly reflective leading the infrared emissivity to decrease sharply. In the third region, the infrared emissivity slightly decreases with increasing Al concentrations from 35 wt. % to 60 wt. %. Infrared emissivity of the coatings slightly decreased from values of 0.385µm to 0.376µm and from values of 0.412µm to 0.387µm at two regions (3-5, 8-12) µm. respectively. Coating was saturated with the filler (Al) and it slightly decreases in emissivity. The perfect percentage for the filler (Al) in the matrix within the range (35 wt. % to 40 wt. %). At high coated Al concentration (35 wt. % Al), the agglomeration of coated Al powder causes non-uniform dispersion, which causes a noticeable increase in surface roughness, which causes an increase in the infrared emissivity. Both theoretically and experimentally, the relationship between emissivity and surface roughness has been investigated [8, 25, 26]. It can be easily represented from equation according to Kirchhoff's law and energy conservation [27].

$$\varepsilon = 1 - \rho_r = 1 - \rho_p \, exp\left(\frac{-4\pi\delta}{\lambda}\right)^2 \qquad (1)$$

Where ρ_r and ρ_p are the reflectance for a rough surface and a polished surface, respectively, δ is surface roughness, ε emissivity and λ is wavelength. Eq. (1) shows that rough-surfaced coatings have a larger infrared emissivity. Where the content of coated Al powder rises 35 wt. %, the negative effect of increased coating surface roughness offsets the emissivity reduction. As a result, the infrared emissivity continues to decrease, but at a slower rate. Although it is not possible to minimize coating emissivity by raising coated Al powder content to extremely high levels, a moderate amount of 35 wt. % is beneficial for the coating's low infrared emissivity and good physical properties [27].

In this section, we fixed the thickness of the coating in the range 13µm to 39µm and fixing speed1 (low speed) at 2, time 18 sec, 0.8*1000 rpm, fixing speed 2 (high speed) at 1, time 20 sec, 1.54*1000 rpm. Thermal signature management takes the form of varying a material's emissivity or adjusting a surface's temperature to effect the quantity of energy radiated from its surface. Figure (9: a-c) illustrates that the thermal signature with various Al content (5%, 20%, 25% 35%, 40%, 60%) at different temperatures (50ºC, 70ºC, 90ºC). The difference between the thermal signatures of Al content is clearly detected in which different temperature ranges are appointed different colors. Table 4 shows the apparent temperature with different Al content.

Table 4. Shows the apparent temperature of different Al content

Al content	T (50 °c)		T (70°c)		T (90°c)	
	°F	°C	°F	°C	°F	°C
5%	107.7	42.0	149.7	65.3	184.8	84.8
20%	104.9	40.5	142.6	61.4	174.9	79.3
25%	101.6	38.6	128.9	53.8	152.4	66.8
35%	100.5	38.0	125.8	52.1	147.4	64.1
40%	99.7	37.6	123.4	50.7	144.1	62.2
60%	99.6	37.5	122.6	50.3	143.4	61.8

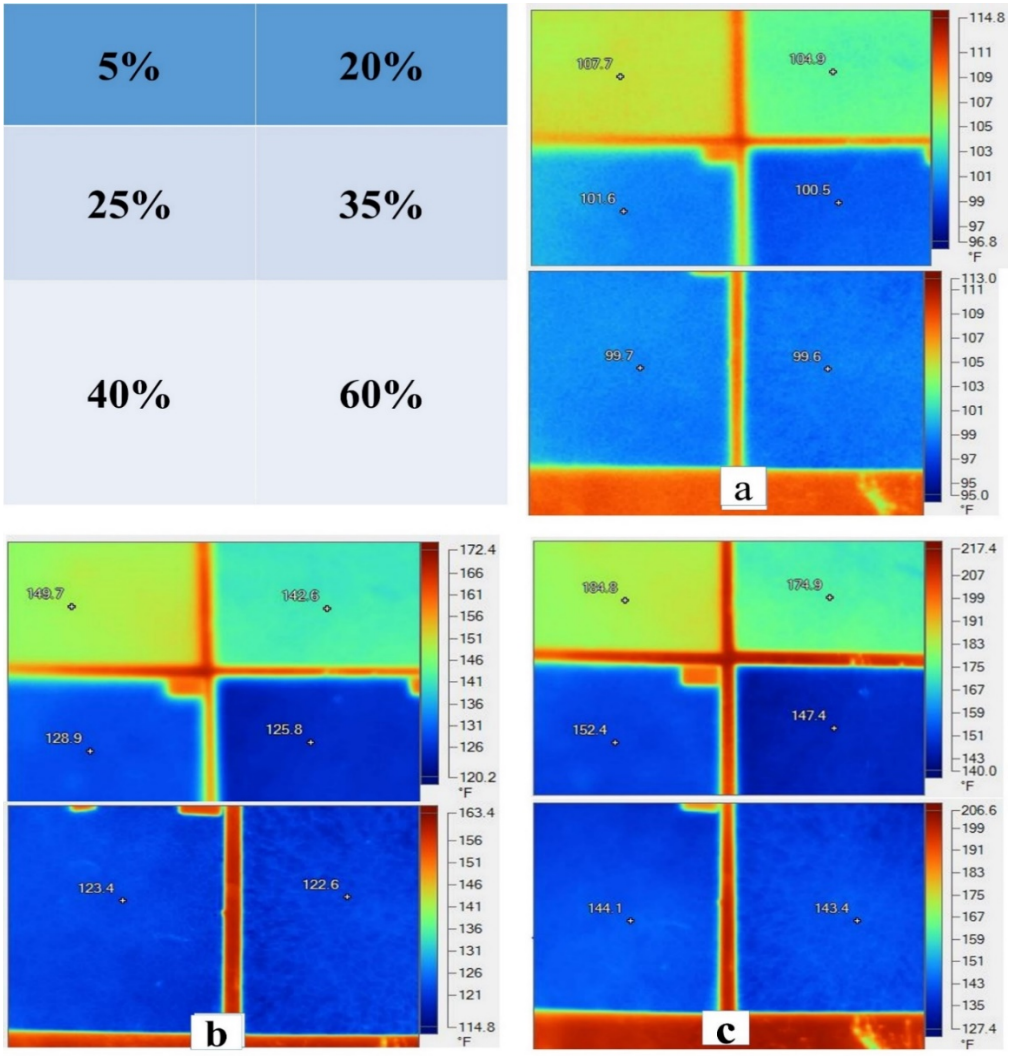

Fig (9: a-c). Shows the thermal signature with various Al content (5%, 20%, 25%, 35%, 40%, and 60%) at different temperature degree (50ºC, 70ºC, 90ºC) for samples 10*10 cm.

As shown from the figure, it confirms the concept of the three regions in fig. (8). At fig. (9: a) with temperature 50cº, increasing Al content from 5 wt.% to 20 wt.% found that the temperature decrease with little percentage from 107.7 Fº to 104.9 Fº where there is difference in temperature equal (2.8 Fº) which is identical with the first region. With successive increasing content from 20 wt.% to 35 wt.%

found that the temperature sharply decreases from 104.9 Fº to 100.5 Fº where there is difference in temperature equal (4.4 Fº) which is nearly double the value than the previous value (2.8 Fº) and typical with the secondly region. With increasing content from 40 wt. %. to 60 wt.%. Found that the temperature slightly decreases from 99.7 Fº to 99.6 Fº where there is difference in temperature equal (0.1 Fº) which is identical with the thirdly region. Finally, the perfect content percentage for the filler (Al) in the matrix with the concentration range from (35 wt. % to 40 wt. %).

4.4.4 Emissivity profile of Nano shape Al powder Figure. (10) Shows the relation between ball milling time, particle size and the infrared emissivity of the coating in two regions band 3-5µm & 8-12µm for Al powder at concentration 30%. The spin coater conditions for Al coatings will be fixed with speed1 (low speed) at 2, time 18 sec, 0.8*1000 rpm and fixing speed 2 (high speed) at 1, time 20 sec, 1.54*1000 rpm. From Figure it can be seen that when milling time increases from 0h to 15h, the average particle sizes decrease from 35µm to 3µm, the infrared emissivity sharply increases from 0.408µm to 0.921µm at region 3-5 µm and sharply increases from 0.429 µm to 0.934µm at region 8-12 µm. By increasing the milling time up to 30h, average particle size is reduced to 300 nm. Therefore, the infrared emissivity slightly increases from 0.921 µm to 0.929µm at region 3-5 and slightly increases from 0.934µm to 0.95µm at region 8-12 µm.

It was found that as the Al particles size reaches the Nano level, the number of particles multiplies dramatically. However, the reunion of Al particles, on the other hand, is seen because the particles are active on the surface of small particles, which reduces successful pigment particle contact and increases porosity. Additionally, higher emissivity may be attributed to high oxidation of Al due to the presence of aluminum oxide (Al_2O_3) with high percent reaches about 39% at corresponding milling time 30h.

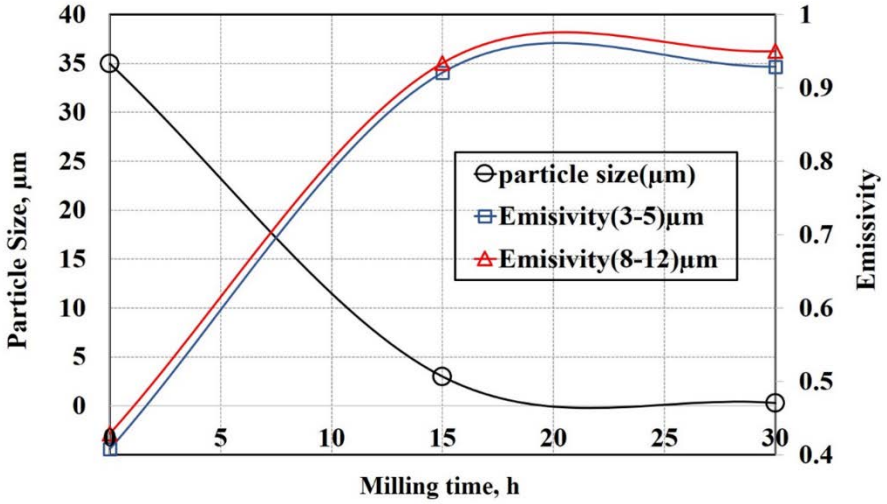

Fig 10. Relation between ball milling time and particle size, infrared emissivity radiation at two regions (3-5, 8-12) µm for Al powder

5. Conclusion

Ball milling approach was utilized to control shape and size of Al powders, which were examined to evaluate their infrared emissivity profiles within the band 3-5 and8-12µm. It was found that particle size has a significant impact on the emissivity of the coatings. Almost Nano Al particles are unfavorable for the formation of low emissivity coatings. On the other hand, the highly flake Al pigments are more suitable for the low infrared emissivity composite coatings. As coat thickness was optimized, it was concluded that the optimum performance achieved 13 µm to 39µm. Furthermore, the optimum Al content to achieve the maximum performance (lowest emissivity) was found to be 35 - 40 wt. %. Moreover, the micro size Al flakes achieves higher performance than the sub micro (Nano size). The formation of Aluminum oxides (Al_2O_3) as results show; due to increase of milling time has a negative impact on emissivity.

References

[1] R. Liu, C. Ji, J. Mock, J. Chin, T. Cui, and D. Smith, 2009 "Broadband ground-plane cloak," *Science,* vol. **323**, pp. 366-69.
[2] L. McDougall, 2012 "*Complete Tracker: Tracks, Signs, and Habits of North American Wildlife*: " Rowman & Littlefield.
[3] C. Mikunda, 2004 "*Brand lands, hot spots & cool spaces: Welcome to the third place and the total marketing experience*: " Kogan Page Publishers.
[4] L. Yuan, X. Weng, and L. Deng, 2013 "Influence of binder viscosity on the control of infrared emissivity in low emissivity coating," *Infrared Physics & Technology,* vol. **56**, pp. 25-29.
[5] P. K. Biswas, A. De, N. Pramanik, P. Chakraborty, K. Ortner, V. Hock, *et al.*, 2003 "Effects of tin on IR reflectivity, thermal emissivity, Hall mobility and plasma wavelength of sol–gel indium tin oxide films on glass," *Materials letters,* vol. **57**, pp. 2326-32.
[6] F.-Y. Zhang, Y.-M. Zhou, Y. Cao, and J. Chen, 2007 "Preparation and characterization of KGM/CdS nanocomposite film with low infrared emissivity," *Materials letters,* vol. **61**, pp. 4811-14.
[7] A. Licciulli, A. Maffezzoli, D. Diso, M. Mazzer, G. Torsello, and S. Tundo, 2004 "Porous garnet coatings tailoring the emissivity of thermostructural materials " *Journal of sol-gel science and technology,* vol. **32**, pp. 247-51.
[8] B. Rousseau, M. Chabin, P. Echegut, A. Sin, F. Weiss, and P. Odier, 2001 "High emissivity of a rough Pr 2 NiO 4 coating," *Applied Physics Letters,* vol. **79**, pp. 3633-35.
[9] G. Leftheriotis and P. Yianoulis, 1999 "Characterisation and stability of low-emittance multiple coatings for glazing applications," *Solar energy materials and solar cells,* vol. **58**, pp. 185-97.
[10] Y. Shan, Y. Zhou, Y. Cao, Q. Xu, H. Ju, and Z. Wu, 2004 "Preparation and infrared emissivity study of collagen-g-PMMA/In2O3 nanocomposite," *Materials letters,* vol. **58**, pp. 1655-60.
[11] L. Fagundes, T. Sousa, A. Sousa, V. Silva, and E. Sousa, 2006 "SBA-15-collagen hybrid material for drug delivery applications," *Journal of non-crystalline solids,* vol. **352**, pp. 3496-01.
[12] G. Wu and D. Yu, 2013 "Preparation and characterization of a new low infrared-emissivity coating based on modified aluminum," *Progress in Organic Coatings,* vol. **76**, pp. 107-12.
[13] C. Hu, G. Xu, X. Shen, C. Shao, and X. Yan, 2010 "The epoxy-siloxane/Al composite coatings with low infrared emissivity for high temperature applications," *Applied surface science,* vol. **256**, pp. 3459-63.
[14] K.-S. Chou and Y.-C. Lu, 2007 "The application of nanosized silver colloids in far infrared low-emissive coating," *Thin Solid Films,* vol. **515**, pp. 7217-21.
[15] H. Chu, Z. Zhang, Y. Liu, and J. Leng, 2016. "Silver particles modified carbon nanotube paper/glassfiber reinforced polymer composite material for high temperature infrared stealth camouflage," *Carbon,* vol. **98**, pp. 557-66.
[16] Y. Xin, H. Zhou, X. Ni, Y. Pan, X. Zhang, J. Zheng, *et al.*, 2015 "The optical properties of low infrared transmittance WO 3− x nanocrystal thin films prepared by DC magnetron sputtering under different oxygen ratios," *RSC Advances,* vol. **5**, pp. 57757-63.
[17] T. Hallberg, T. Heikkila, H. Karlsson, P. S. Salonen, C. Nilsson, and A. Janis, 2005 "*Development of low-emissive camouflage paint*: Sensor Technology", Swedish Defence Research Agency.
[18] L. E. Nunes Almeida, A. Martins, S. R. Gomes, S. Aramaki, R. O. Pinto, and F. Cunha, 2013 "Infrared Camouflage of the Warfighter's Equipment through Enhanced Coating Technology," in *49th AIAA/ASME/SAE/ASEE Joint PropulsionConference*, ed, p. 4101.
[19] R. F. Supcoe, 1982 "Blue-gray low infrared emitting coating," ed: Google Patents.
[20] W. Mazurczyk, S. Wendzel, S. Zander, A. Houmansadr, and K. Szczypiorski, 2016 "*Information hiding in communication networks: fundamentals, mechanisms, applications, and countermeasures*": John Wiley & Sons.
[21] Kim, T., Bae, J.Y., Lee, N. and Cho, H.H., 2019. Hierarchical metamaterials for multispectral camouflage of infrared and microwaves. *Advanced Functional Materials*, ***29*(10)**, p.1807319.

[22] J. R. White, 2012 "Aircraft infrared principles, signatures, threats, and countermeasures," NAVAL AIR WARFARE CENTER WEAPONS DIV CHINA LAKE CA.
[23] B. W. Krueger, C. S. Dandeneau, E. M. Nelson, S. T. Dunham, F. S. Ohuchi, and M. A. Olmstead, 2016 "Variation of Band Gap and Lattice Parameters of β−(AlxGa1− x) 2O3 Powder Produced by Solution Combustion Synthesis," *Journal of the American Ceramic Society,* vol. **99**, pp. 2467-73.
[24] C. Wu, H. Tan, W. Huang, W. Li, K. N. Dinh, C. Yan, *et al.*, 2020 "A new scalable preparation of metal nanosheets: potential applications for aqueous Zn ion batteries anode," Advanced *Functional Materials,* vol. **30**, p. 2003187.
[25] F. Ghmari, T. Ghbara, M. Laroche, R. Carminati, and J. J. Greffet, 2004 "Influence of microroughness on emissivity," *Journal of Applied Physics,* vol. **96**, pp. 2656-64.
[26] J. O. Sacadura, 1972 "Influence de la rugosité sur le rayonnement thermique émis par les surfaces opaques: Essai de modèle," *International Journal of Heat and Mass Transfer,* vol. **15**, pp. 1451-65.
[27] G. Wu and D. Yu, 2012 "Preparation of a novel infrared low-emissive coating from the Cu powder modified by the polyethylene wax," *Infrared Physics & Technology,* vol. **55**, pp. 26-31.